SEISMIC RESPONSE ANALYSIS OF MILAD TOWER IN TEHRAN, IRAN, UNDER SITE-SPECIFIC SIMULATED GROUND MOTIONS

H. Zafarani[1], A.K. Ghorbani-Tanha[2], M. Rahimian[3] and A. Noorzad[4]

[1] *PhD Graduate, School of Civil Engineering, University of Tehran, Tehran, Iran*
[2] *Assistant Professor, School of Civil Engineering, University of Tehran, Tehran, Iran*
[3] *Associate Professor, School of Civil Engineering, University of Tehran, Tehran, Iran*
[4] *Assistant Professor, School of Civil Engineering, University of Tehran, Tehran, Iran*

hamzafarani@yahoo.com, ghtanha@ut.ac.ir, rahimian@ut.ac.ir, noorzad@ut.ac.ir

ABSTRACT

With a height of 435 m, Milad tower would be the fourth highest TV and telecommunication tower of the world. The tower is situated in north-west of Tehran, few kilometers from the known “North Tehran” and “Ray” active faults. Therefore, taking into account the near field aspects of strong motion in the design of such an important structure is necessary. In present study, time histories at the tower’s site, for different scenario earthquakes along the nearest sources are simulated using the stochastic finite-fault simulation method of Beresnev and Atkinson (1997, 1998). The stick model for the tower is constructed and the effects of different fault rupture scenario on the response of the structure under simulated earthquake excitations are investigated. We have explored the sensitivity of the results to the variation of the nucleation point, so, all other parameters such as the stress drop and strength radiation factor are assumed at their best estimate values. For each fault model, three different nucleation points is considered and the resultant motions are generate using a random slip distribution on the fault plane. The results show that changing the nucleation point results in the variation of the response of the tower more than hundred percent in some cases. The computed acceleration time histories and response spectra would be the most useful tools for design engineers and the results of the seismic response analyses enables designer to have a better insight into the overall response of the tower during the most expected seismic motions.

KEYWORDS:

Milad Tower, Stochastic Simulation of Ground Motion, Finite-Fault Method, Fault Rupture Characteristics

1. INTRODUCTION

With a height of 435 m, Milad Tower, situated in north-west of Tehran, is the fourth highest telecommunication tower of the world (Figure 1). This multi-purpose tower will provide communication, broadcasting, wireless access, Aerology, traffic control, etc. facilities. It consists of foundation, base building (lobby), main shaft, head structure, and antenna mast. The main shaft consists of a central shaft and four legs. The central shaft consists of two nested octagons. The legs with varying hollow trapezoidal sections disappear at the level of 240 m so that the main shaft has the diameter of 28 m at zero level and decreases to 17 m at the level of 240 m. The central shaft extends up to the level of 315 m. The head structure of the tower extends from the level of 247.5 m to 315 m. A steel 120 m high antenna mast extends from the top of head structure up to the level of 435 m. The tower is located in the vicinity of several active faults. The closest faults are the North Tehran, Ray and Mosha faults. As a result, accurate prediction of future earthquakes and ground motion characteristics is necessary for such especially important structure. The most important step in seismic hazard analysis is to calculate the peak ground accelerations (PGA) and frequency contents of motions which can affect a site. In the current procedure of probabilistic seismic hazard analysis (PSHA), these parameters are determined from empirical attenuation equations, which are formulated as functions of distance and earthquake magnitude.

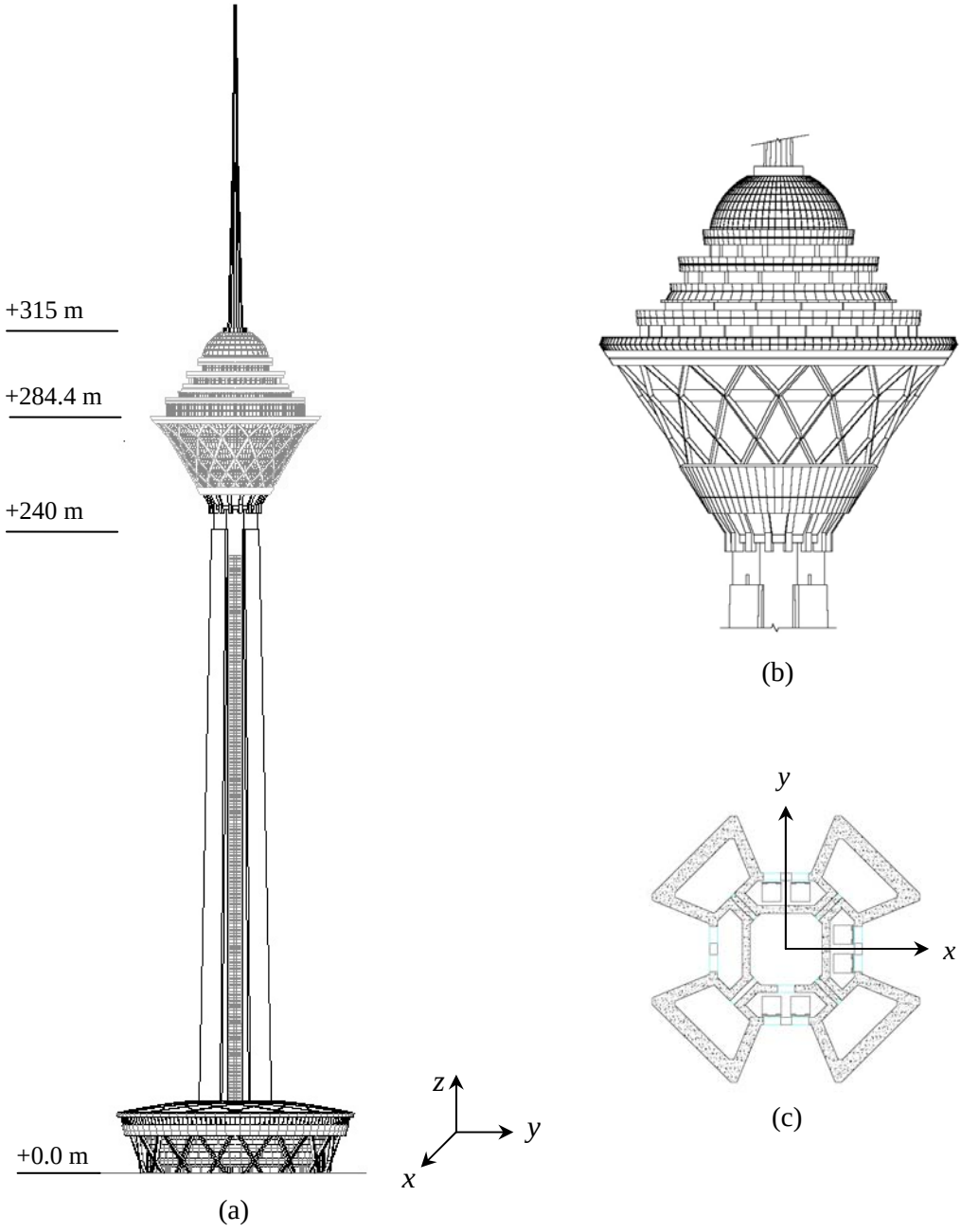

Figure 1. Milad Tower: (a) Configuration; (b) Head structure; (c) Shaft section at zero level.

Unfortunately, in near-fault regions (at a distance of about 10 km, or a few wavelengths) where the number of records of large earthquakes is usually inadequate, these equations show a large uncertainty which cannot be improved unless sufficient data become available. Now a better procedure for major structures located near active faults is to carry out theoretical simulations to capture the main aspects of ground motion near the seismic sources. Simulation methods, referred to also as the 'physical methods'; are also the preferred approach of seismic hazard evaluation for regions such as Tehran where strong motion data is sparse and the late earthquake dates back to the pre instrumental era (Zafarani *et al*., 2008, 20xx).

The purpose of this study is to investigate the effects of different fault rupture scenarios on the response of the Milad Tower under simulated earthquake excitations. In this study, we use the stochastic finite-fault simulation technique of Beresnev and Atkinson (1997, 1998) which implements the concept of fault discretization wherein sub-events are represented as stochastic point sources. The applied finite-fault approach allows one to define

independently a variety of rupture scenarios on the fault plane by varying the hypocenter location, rupture velocity, fault plane geometry, slip distribution and stress drop. Recently, Zafarani *et al*. (20xx) has calibrated the model for Iranian earthquakes and also has proposed an empirical relationship for the strength radiation factor (*sfact*), which is the most important parameter of the model and controls the high frequency radiation from the source. Their preferred scenarios are used in this study to generate the most favorable strong motions that may affect the tower.

In order to more highlight the importance of simple aspects of strong motion generation such as directivity effect and nucleation point, all other parameters such as the stress drop and *sfact* are assumed at their best estimate values. For each fault model, three different nucleation points are considered and the resultant motions are generated using a random slip distribution on the fault plane. The dynamic analyses of the structure subjected to the simulated earthquake records are conducted. The results are reported and comparisons are made to demonstrate the effects of fault rupture scenarios on the structural response.

2. SEISMICITY OF TEHRAN REGION

Tehran is located in the Alborz Seismic Zone (ASZ). The probability of occurrence of a large earthquake ($M > 6.5$) within a circular area of 150 km around Tehran, in the next 100 years, has estimated to be 0.65 (Yadman Sazeh Corporation, 2002). A large earthquake in the ASZ is likely to cause great loss of life and severe damage to construction in and near the epicentral zone. The most important population area is Tehran, a city of more than eight million inhabitants, lies in the vicinity of some major active faults in the ASZ. Unfortunately, the sparse strong-motion data set presently available from existing faults in Tehran area makes the estimation of ground motion during future earthquakes quite a challenge. Tehran is close to the Mosha (MF), North Tehran (NTF), North Ray (NRF), South Ray (SRF), Kahrizak and Parchin (also referred to as Eyvanaki) active reverse faults. The area has been affected by a number of destructive historical earthquakes in the past years. The magnitudes of these earthquakes are listed in Table 1 (Ambraseys and Melville, 1982; Berberian *et al.*, 1983). From geologic and historical seismicity evidence it is inevitable that a large earthquake will strike the Tehran region sooner or later. In order to prepare for this eventuality, it is critical to quantify the effects of such a scenario. In the absence of sufficient strong motion data, the only option is to use physical simulations for this purpose.

Table 1. Historical seismicity of ASZ around Tehran

Date	M_S	Associated Fault*	Epicenter E°	Epicenter N°
312-281 BC	~7.6	?	51.8	35.5
AD 743	~7.2	?	52.2	35.3
AD 855	~7.1	SRF or NRF	51.5	35.6
AD 864	>5.3	?	51.0	35.7
AD 958	~7.7	NTF or MF	51.1	36.0
AD 1177	~7.2	NTF	50.7	35.7
AD 1665	~6.5	MF	52.1	35.7
AD 1830	~7.1	MF	52.5(51.7)**	35.7(35.8)

*Based on Berberian *et al*. (1983) and Berberian and Yeats (1999).
**The value in parentheses is location of this event according to Berberian and Yeats (1999).

The Mosha fault is over 200 km long, and consists of several segments. According to Berberian and Yeats (1999), at least three damaging historical earthquakes ruptured adjacent segments of the Mosha fault for a continuous distance of nearly 200 km: 958 (western segment), 1665 (eastern segment), and 1830 (central segment, north of Tehran). The NRF and SRF are located on the south border of Tehran city. The length of these faults is about 20 km. We believe, following Moinfar *et al*. (2002), that the root of NRF and SRF is the same and these are branches of one fault, so we define a representative fault model of both faults referred to as the Ray Fault Model. Thus, three active faults have been considered as potential sources of hazard at Tehran in this study. The NTF lies on the boundary between the northern mountainous area and the city area. This fault which extends over 75 km consists

of two main segments: North-western and eastern parts (Berberian *et al*., 1983). North-western segment is far from the city and so the eastern part was selected as a potential source of one of the scenario earthquakes. Future earthquake events from rupture scenarios along the three major faults are considered as delineated in Figure 2.

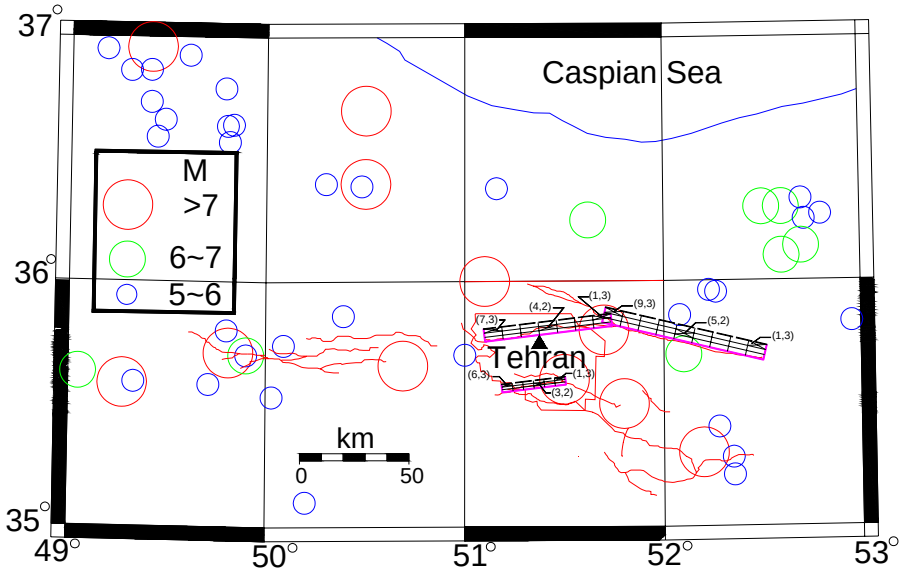

Figure 2. Historical earthquakes around Tehran. The projection of the fault models are also shown, as well as the approximate location of the fault traces. Thick line indicates projection of the top edge of the fault. The fault areas are divided in $i \times j$ subfaults. The rupture initiates in the subfault (i_0, j_0). Milad Tower is also shown with a solid triangle.

3. SIMULATION METHOD AND SELECTED SCENARIOS

In the near-source region of large earthquakes, aspects of a finite-source including rupture propagation, directivity, and source-receiver geometry can be significant and may be incorporated into strong ground motion predictions. To accommodate these effects, a methodology that combines the aspects of finite-fault modeling techniques (Hartzell, 1978) with the stochastic point-source ground motion model (Boore, 2003) has been developed by Beresnev and Atkinson (1997, 1998) to produce response spectra as well as time histories appropriate for engineering application.

According to Beresnev and Atkinson (2002), the fault plane is divided in subfaults whose size, Δl, in km, increases linearly with moment magnitude, in accordance with the relationship

$$\log \Delta l = -2 + 0.4\, M \quad (4 \le M \le 8) \tag{1}$$

These authors have derived this relationship for both west and east North America, and concluded that it is a relationship which is not specific to any region, hence we have determined the sub-fault size in our simulations from this equation, taking into account that it has been implemented successfully for such simulations in other parts of the world (Zafarani *et al*., 20xx).

The subfaults are stochastic ω^2 sources. The subevent time history at a site is generated following the procedure of Boore (2003). The rupture propagates radially from a specified hypocenter. A standard technique sums the contribution from each subfault. Randomness is introduced in the subevent rupture times. A free parameter, called the strength factor, which is the parameter controlling the level of high-frequency radiation in the simulated spectra and reflects the maximum slip velocity on the fault, needs to be specified (see Beresnev and Atkinson (1997, 1998)).

Recently, Zafarani *et al*. (20xx) has determined *sfact* for eight Iranian earthquakes, based on an event-by-event approach, by fitting simulated to observed response spectra. In the present study, we used the best estimate scenarios of Zafarani *et al*. (20xx) in order to simulate strong motions. A stress parameter, which relates subfault moment and its size, is fixed at 50 bars. All sites are assumed to contain the generic rock amplification described by Mousavi *et al*. (2007).

A random distribution of slip on the fault plane was assumed in all simulations by specifying a random seed number. The generic regional parameters which are fixed for all simulations are listed in Table 2.

Table 2. Model parameters used for Tehran region

Parameter	Parameter value
Stress parameter (bars)	50
Crustal shear-wave velocity (km/sec)	3.5
Rupture velocity (km/sec)	0.8 × shear-wave velocity
Crustal density (g/cm^3)	2.8
$Q(f)$	$Q(f)=291\,f^{0.6}$ (Motazedian, 2006)
Path duration	$0.1r$
Windowing function	Saragoni-Hart
Geometric spreading	R^{-1}($R \le 60$ km), $R^{-1/2}$($R > 60$ km) (Motazedian, 2006)
Crustal amplification	Mousavi *et al.* (2007)
Kappa (parameter of high-cut filter, sec)	0.05 (Motazedian, 2006)

In the absence of recurrence interval of selected faults, the worst case scenario that would result from each fault (M_{max}) is calculated based on both the historical data and the empirical relationships between magnitude and fault length and width (Wells and Coppersmith, 1994).

For the Mosha fault we assume that the rupture length can reach up to about 37% of the fault length (Tavakoli and Ghafori-Ashtiany, 1999). Therefore, this fault is capable of generating earthquakes up to a magnitude of 7.4. For the North Tehran fault we believe a value of M_{max} 7.2 because some historical evidence suggests that the 1177 AD earthquake has been associated with the rupture of this fault (Berberian and Yeats, 1999). This scenario involves the rupture of a 58-km segment of the North Tehran Fault. This means that the whole length of eastern segment is modeled. There is some ambiguity about the true location of the 855 earthquake. Because of the poor documentation, the 855 earthquake could be mislocated, although there is a suggestion that the event has been located along the Ray-Kahrizak fault system south of Tehran (Berberian and Yeats, 1999). In this study following Moinfar *et al*. (2002), we assume that the whole length of this fault could rupture and assign a value of M_{max} 6.7 to it.

The strike and the dip angles of the faults are similar to the values chosen by Moinfar *et al*. (2002) for Mosha, Ray and North Tehran faults, respectively, using data from the surface traces and microseismicity studies. The information on selected scenario earthquakes on each fault and its dimensions are tabulated in Table 3. The strength factor, *sfact*, needs to be specified for each earthquake scenario. The values of desired magnitudes in Eqn. 4 of Zafarani *et al*. (20xx) resulted in *sfact* values tabulated in Table 3.

Table 3. Scenario earthquakes and dimensions of each fault

Fault	Mw	Strike/Dip	Origin		Length (km)	Width (km)	Depth to top of fault (km)	*sfact*
			E^o	N^o				
Mosha	7.4	283^o/75^o	52.4955	35.6815	75	27	1	1.4
Ray	6.7	263^o/75^o	51.5061	35.5876	29	14	6	1.5
North Tehran	7.2	263^o/75^o	51.7392	35.8255	58	22	2	1.5

4. EQUATIONS OF MOTION OF THE STRUCTURE

Because of its symmetry and high slenderness ratio, Milad Tower is modeled as a vertical linear cantilever beam, refered to as 'stick model', with 57 translational and 57 rotational degrees of freedom (DOFs). In order to reduce the computational effort, Guyan reduction method is employed to eliminate those DOFs associated primarily with higher modes, i.e. 57 rotational DOFs (Guyan, 1965). The information concerning Milad Tower together with the details of the reduction procedure is provided in Ghorbani-Tanha *et al.* (2005). The only difference is that, herein, the mass of the structure is idealized as lumped or concentrated at nodes or, in other word, a lumped-mass matrix is used. The reduced equation of motion of the tower is

$$\mathbf{M}\ddot{\mathbf{X}}(t)+\mathbf{C}\dot{\mathbf{X}}(t)+\mathbf{K}\mathbf{X}(t)=-\mathbf{M}\mathbf{r}\ddot{u}_g(t) \tag{4.1}$$

where **M**, **C**, and **K** are $n\times n$ mass, damping, and stiffness matrices respectively $(n=57)$; $\mathbf{X}(t)=[x_1(t),\ x_2(t),\ ...,\ x_n(t)]^T$ is an n displacement vector with $x_i(t)$, $i=1,\ ...,\ n$, being the displacement of the ith DOF of the tower and ^{T} denoting vector transpose; $\ddot{u}_g(t)$ is the ground acceleration; **r** is an n element unit vector and a dot denotes differentiation with respect to time. Eqn. 4.1 can be expressed in state space as

$$\dot{\mathbf{z}}(t)=\mathbf{A}\mathbf{z}(t)+\mathbf{B}\ddot{u}_g(t) \tag{4.2}$$

where $\mathbf{z}(t)$ is n element state vector; **A** is $2n\times 2n$ system matrix; **B** is $2n\times 1$ external excitation location vector given, respectively, by

$$\mathbf{z}(t)=\begin{bmatrix}\mathbf{X}(t)\\ \dot{\mathbf{X}}(t)\end{bmatrix};\quad \mathbf{A}=\begin{bmatrix}\mathbf{0} & \mathbf{I}\\ -\mathbf{M}^{-1}\mathbf{K} & -\mathbf{M}^{-1}\mathbf{C}\end{bmatrix};\quad \mathbf{B}=-\begin{bmatrix}\mathbf{0}_{n\times 1}\\ \mathbf{r}\end{bmatrix} \tag{4.3}$$

where **0** and **I** are $n\times n$ zero and identity matrices, respectively, and $\mathbf{0}_{n\times 1}$ is is an n element zero vector.

5. NUMERICAL RESULTS

Simulated time histories for different scenarios along the Mosha, North Tehran and Ray faults are provided, respectively, in Figures 4-6. In each figure three different time histories are available which are obtained according to the assumed location of the hypocenter as mentioned in the figure caption and was shown in Figure 2.

Structural analyses have been carried out by means of the finite element method. The computed first four natural frequencies of the tower are 1.09, 3.60, 5.66, 11.50 rad/sec. Since the tower is flexible, it has long natural period and quite low damping (Ghorbani-Tanha *et al*. 2005, 20xx). In present study, the tower is assumed to be undamped.

In order to investigate the effects of variation of the nucleation point on the response of the tower, dynamic analysis of the structure excited by the simulated earthquake time histories are conducted. The maximum (MAX) and normed or root mean square (RMS) displacement response quantities of the tower with respect to the ground are presented in Tables 4-6. These values are reported for six points which are located, respectively, in the middle of the shaft (145 m), in the bottom, middle and top of the head structure (245, 280 and 305 m), and in the upper parts of the antenna mast (415.3 and 435 m). The norm is calculated by the following relation

$$\|\cdot\|=\sqrt{\frac{1}{t_f}\int_0^{t_f}\|\cdot\|^2\,dt} \tag{5.1}$$

where t_f is the duration of the time history of the earthquake used.

The results show that changing the nucleation point results to the variation of the response of the tower more than hundred percent in some cases.

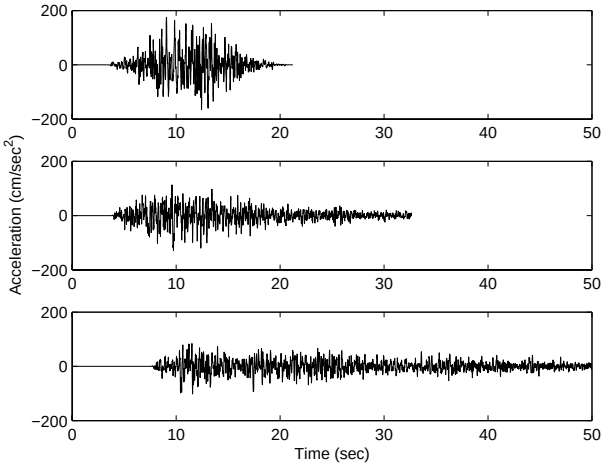

Figure 3. Simulated time histories for different scenarios along the Mosha fault, hypocenter at subfault (1,3): top frame; hypocenter at subfault (5,2): mid frame; hypocenter at subfault (9,3): bottom frame.

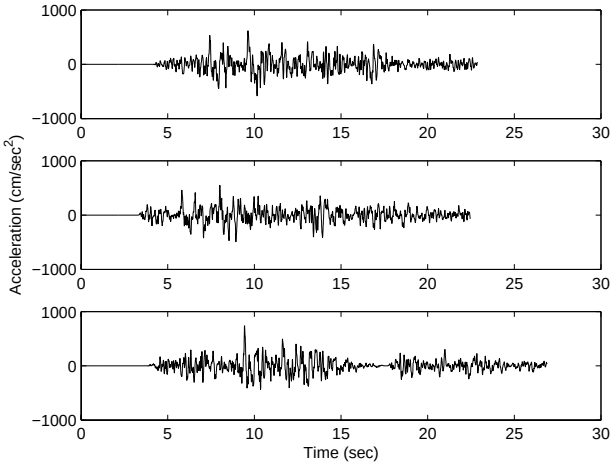

Figure 4. Simulated time histories for different scenarios along the North Tehran fault, hypocenter at subfault (1,3): top frame; hypocenter at subfault (4,2): mid frame; hypocenter at subfault (7,3): bottom frame.

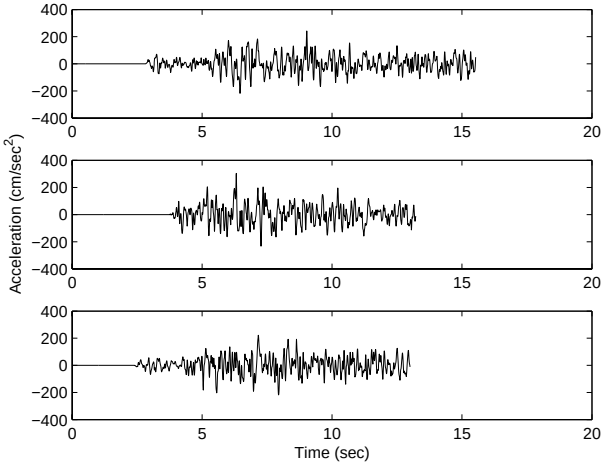

Figure 5. Simulated time histories for different scenarios along the Ray fault, hypocenter at subfault (1,3): top frame; hypocenter at subfault (3,2): mid frame; hypocenter at subfault (6,3): bottom frame.

Table 4. Displacement response quantities of the tower for the simulated records of Mosha fault

	Mosha (1,3)		Mosha (5,2)		Mosha (9,3)	
Level (m)	MAX Displacement (m)	RMS Displacement (m)	MAX Displacement (m)	RMS Displacement (m)	MAX Displacement (m)	RMS Displacement (m)
145	0.04	0.01	0.06	0.02	0.06	0.03
245	0.06	0.02	0.04	0.02	0.05	0.02
280	0.08	0.02	0.05	0.02	0.06	0.02
305	0.11	0.03	0.09	0.03	0.10	0.04
415.3	0.58	0.14	0.90	0.33	0.83	0.25
435	1.59	0.42	1.89	0.55	1.70	0.49

Table 5. Displacement response quantities of the tower for the simulated records of North Tehran fault

	North Tehran (1,3)		North Tehran (4,2)		North Tehran (7,3)	
Level (m)	MAX Displacement (m)	RMS Displacement (m)	MAX Displacement (m)	RMS Displacement (m)	MAX Displacement (m)	RMS Displacement (m)
145	0.48	0.19	0.34	0.14	0.39	0.15
245	0.43	0.16	0.27	0.09	0.39	0.15
280	0.61	0.21	0.29	0.11	0.47	0.19
305	0.93	0.30	0.50	0.18	0.77	0.26
415.3	3.51	1.20	2.77	0.94	2.95	1.02
435	8.13	2.48	6.50	2.06	10.29	2.45

Table 6. Displacement response quantities of the tower for the simulated records of Ray fault

	Ray (1,3)		Ray (3,2)		Ray (6,3)	
Level (m)	MAX Displacement (m)	RMS Displacement (m)	MAX Displacement (m)	RMS Displacement (m)	MAX Displacement (m)	RMS Displacement (m)
145	0.13	0.05	0.12	0.05	0.12	0.04
245	0.10	0.04	0.15	0.07	0.10	0.03
280	0.14	0.05	0.20	0.08	0.14	0.04
305	0.23	0.08	0.24	0.10	0.22	0.07
415.3	1.12	0.33	1.21	0.37	0.89	0.28
435	2.77	0.73	2.50	0.74	2.10	0.57

6. CONCLUSIONS

In this study, to give some idea of the sensitivity of the response of the Milad Tower to the variation of nucleation point, all other source parameters are kept at their best estimate values. It should be noted that all of these potential scenarios are deterministic ones and are actually the Maximum Credible Earthquakes (MCEs) that may affect the site. As it is clear, changing the nucleation point while keeping all other parameters constant has a clear effect on the results up to more than hundred percent in some cases. Also, as it was expected, the most dramatic effect on the tower is due to the North Tehran fault scenarios which are the closest one to the site. Ray and Mosha fault stand in the next degrees of importance, respectively.

From the engineering seismology point of view, the result show that precise description and estimation of the effective parameters in generation of strong motion such as fault type, desired earthquake magnitude, stress drop, and characteristics of fault rupture is of great importance. The improvement of numerical simulation techniques and knowledge of source processes and underground structure are needed for the development of more realistic scenarios. Note that different seed numbers should be used to simulate synthesized earthquake records for each scenario earthquake to consider the uncertainty effects (path and source effects) which results in the generation of

high frequency parts of motion. In present study only one synthesized time history is generated for each set of parameters. The applied finite-fault method includes the salient features of high frequency ground motion and the fault and site geometry aspects. However, this method fails to describe long period pulse-like aspects of near-fault ground motions. Taking into account the flexibility of this high rise structure and its high dominant vibration period, it is necessary to use a hybrid procedure, which combines both long period pulse features (not seen in the finite-fault method) and high frequency components in the near-fault ground motions, for the assessment of design basis earthquake ground motions.

REFERENCES

Ambraseys, N.N. and Melville, C.P. (1982). A History of Persian Earthquakes, Cambridge University Press, London.

Berberian, M., Qorashi, M., Arzhang-ravesh, B. and Mohajer-Ashjai, A. (1983). Recent Tectonics, Seismotectonics and Earthquake-Fault Hazard Investigation in the Greater Tehran Region: Contribution to the Seismotectonics of Iran, Part V. Geological Survey of Iran, Report No. 56.

Berberian, M. and Yeats, R.S. (1999). Patterns of historical earthquake rupture in the Iranian plateau. *Bulletin of the Seismological Society of America* **89**, 120–139.

Berberian, M. and Yeats, R.S. (2001). Contribution of archaeological data to studies of earthquake history in the Iranian plateau. *Journal of Structural Geology* **23**, 563–584.

Beresnev, I. A. and Atkinson, G.M. (1997). Modeling finite-fault radiation from the omega-n spectrum. *Bulletin of the Seismological Society of America* **87**, 67-84.

Beresnev, I. A. and Atkinson, G.M. (1998). FINSIM: a FORTRAN program for simulating stochastic acceleration time histories from finite faults. *Seismological Research Letters* **69**, 27–32.

Beresnev, I. A. and Atkinson, G.M. (2002). Source parameters of earthquakes in eastern and western north America based on finite-fault modeling. *Bulletin of the Seismological Society of America* **92**, 695–710.

Boore, D. M. (2003). Simulation of ground motion using the stochastic method. *Pure and Applied Geophysics* **160**, 635-676.

Ghorbani-Tanha, A.K., Rahimian, M. and Noorzad, A. (2005). Dynamic response of Milad Tower in Tehran, Iran, under wind excitation, *The 7th International Conference on Multi-Purpose High Rise Towers and Tall Buildings*, Dec. 10-11, 2005, Dubai, UAE, Paper IFHS-106. (CD-ROM, 8 pages)

Ghorbani-Tanha, A.K., Noorzad, A. and Rahimian, M. (20xx). Mitigation of wind-induced motion of Milad Tower by tuned mass damper, Accepted for publication in *The Structural Design of Tall and Special Buildings*.

Guyan, R.J. (1965). Reduction of stiffness and mass matrix. *AIAA Journal* **3**, 380.

Hartzel, S.H. (1978), Earthquake aftershocks as Green's functions. *Geophysical Research Letters* **5**, 1-4.

Moinfar, A.A., Naderzadeh, A. and Naiieri, A. (2002). Development of scenario earthquakes for the seismic microzoning of Tehran. *Proceedings of 12th European Conference on Earthquake Engineering*, Sep. 9-13, 2002, London, Paper 204.

Mousavi, M., Zafarani, H., Noorzad, A., Ansari, A. and Bargi, K. (2007). Analysis of Iranian strong-motion data using the specific barrier model. *Journal of Geophysics and Engineering* **4**, 415-428.

Motazedian, D. (2006). Region-specific key seismic parameters for earthquakes in Northern Iran. *Bulletin of the Seismological Society of America* **96**, 1383–95.

Tavakoli, B. and Ghafory-Ashtiany, M. (1999). Seismic hazard assessment of Iran. *Annali Di Geofisica* **42**, 1013-1021.

Wells, D. and Coppersmith, K. (1994). New empirical relationships among magnitude, rupture length, rupture width, rupture area, and surface displacement. *Bulletin of the Seismological Society of America* **84**, 974–1002.

Yadman Sazeh Corporation (2002). Report on Seismicity, Seismotectonic and Seismic Hazard Analysis of Milad Tower – Final Report, Tehran, Iran.

Zafarani, H., Mousavi, M., Noorzad, A. and Ansari, A. (2008). Calibration of the specific barrier model to Iranian plateau earthquakes and development of physically based attenuation relationships for Iran. *Soil Dynamics and Earthquake Engineering* **28**, 550-576.

Zafarani, H., Noorzad, A., Ansari, A. and Bargi, K. (200x). Stochastic modeling of Iranian earthquakes and estimation of ground motion for future earthquakes in Greater Tehran. Accepted for publication in *Soil Dynamics and Earthquake Engineering*.